Journal of Biomedical Optics

SPIEDigitalLibrary.org/jbo

Structural alterations in rat liver proteins due to streptozotocin-induced diabetes and the recovery effect of selenium: Fourier transform infrared microspectroscopy and neural network study

Ozlem Bozkurt
Sevgi Haman Bayari
Mete Severcan
Christoph Krafft
Jürgen Popp
Feride Severcan

SPIE

Structural alterations in rat liver proteins due to streptozotocin-induced diabetes and the recovery effect of selenium: Fourier transform infrared microspectroscopy and neural network study

Ozlem Bozkurt,[a] Sevgi Haman Bayari,[b] Mete Severcan,[c] Christoph Krafft,[d] Jürgen Popp,[d,e] and Feride Severcan[a]
[a]Middle East Technical University, Department of Biological Sciences, 06800 Ankara, Turkey
[b]Hacettepe University, Department of Physics Education, Faculty of Education, Beytepe 06800 Ankara, Turkey
[c]Middle East Technical University, Department of Electrical and Electronics Engineering, 06800 Ankara, Turkey
[d]Institute of Photonic Technology, Albert-Einstein-Str. 9, 07745 Jena, Germany
[e]University Jena, Institute of Physical Chemistry, Helmholtzweg 4, 07743 Jena, Germany

Abstract. The relation between protein structural alterations and tissue dysfunction is a major concern as protein fibrillation and/or aggregation due to structural alterations has been reported in many disease states. In the current study, Fourier transform infrared microspectroscopic imaging has been used to investigate diabetes-induced changes on protein secondary structure and macromolecular content in streptozotocin-induced diabetic rat liver. Protein secondary structural alterations were predicted using neural network approach utilizing the amide I region. Moreover, the role of selenium in the recovery of diabetes-induced alterations on macromolecular content and protein secondary structure was also studied. The results revealed that diabetes induced a decrease in lipid to protein and glycogen to protein ratios in diabetic livers. Significant alterations in protein secondary structure were observed with a decrease in α-helical and an increase in β-sheet content. Both doses of selenium restored diabetes-induced changes in lipid to protein and glycogen to protein ratios. However, low-dose selenium supplementation was not sufficient to recover the effects of diabetes on protein secondary structure, while a higher dose of selenium fully restored diabetes-induced alterations in protein structure. [DOI: 10.1117/1.JBO.17.7.076023]

Keywords: diabetes; liver; selenium; protein structure; Fourier transform infrared imaging; Fourier transform infrared microspectroscopy; neural networks.

Paper 12107 received Feb. 13, 2012; revised manuscript received Jun. 21, 2012; accepted for publication Jun. 22, 2012; published online Jul. 17, 2012.

1 Introduction

In recent years research has been focused on the association between protein conformation and generation of diseases. Protein secondary structural alterations leading to the aggregation of proteins have been identified as protein conformational diseases, such as Alzheimer's, Parkinson's, and prion diseases.[1,2] The protein deposits observed in these diseases interfere with tissue functioning and induce toxicity in cells. Researchers have also identified amyloid protein deposits with altered structure in the pancreatic tissues of type II (non-insulin dependent) diabetic subjects; therefore type II diabetes mellitus (DM) can also be considered as a protein conformational disease.[3,4] Limited number of studies have also indicated that there are changes in protein structure in type I (insulin dependent) DM in different tissues and membranes.[5–8]

DM is a major endocrine disorder and a growing health problem in the world, characterized by hyperglycemia resulting from inadequate insulin secretion and/or diminished tissue responses to insulin. As it causes abnormalities in carbohydrate, fat, and protein metabolism, DM affects nearly all of the organs and systems in the body.[5–15] As a result of the altered metabolic state in DM, many tissue-specific cells are continuously subjected to insult from reactive oxygen species (ROS).[16] The generation of ROS in an uncontrolled fashion causes significant reversible or irreversible damage to a wide range of biological molecules, which can be used in the classification and diagnosis of the disease, even at very early stages.[6,17] The overproduction of ROS in tissues is generally counterbalanced by the activity of enzymes in the antioxidant defense system, such as superoxide dismutase and glutathione peroxidases (GSH-Px). Liver is the central organ for the control of metabolism and glucose homeostasis in the body, as it houses some key enzymes in lipid, carbohydrate, and protein metabolism and reported to be one of the tissues most affected from the oxidative stress conditions in DM.[12]

Being a part of the redox-active center of functional selenoproteins, such as GSH-Px and thioredoxin reductases,[18,19] selenium is an essential trace element that plays an important role in antioxidant defense mechanism of the body. Supplementation of selenium was reported to be beneficial in the prevention of cardiovascular and neurodegenerative diseases, delay of aging, functioning of the immune system, and prevention of certain forms of cancer.[20–22] Although it was reported to have insulin-mimetic and antidiabetic action for many years in animal studies,[9,18,23] recent epidemiological research demonstrated that

Address all correspondence to: Feride Severcan, Middle East Technical University, Department of Biological Sciences, 06800 Ankara, Turkey. Tel: + 90-312-210-51-66; Fax: + 90-312-210-79-76; E-mail: feride@metu.edu.tr

0091-3286/2012/$25.00 © 2012 SPIE

persistent high serum levels of selenium may increase the risk of developing type II DM and hyperlipidemia.[24–26]

Pathological conditions cause alterations in macromolecular properties in tissues, which can be successfully monitored by Fourier transform infrared (FTIR) spectroscopy and microscopy.[27–30] These vibrational spectroscopic techniques are becoming increasingly powerful and efficient tools to analyze protein secondary structural alterations[31] and have exhibited their increasingly important role in the field of characterization of several diseases,[6–8,11,32–35] even in the early stages.

In the current study, the changes in protein secondary structure and macromolecular content of type I diabetic rat liver tissues were investigated for the first time in comparison with healthy rat liver tissues using FTIR microspectroscopy. In addition, the role of selenium in the recovery of diabetes-induced alterations in rat liver tissues was studied. Protein secondary structure was determined by neural network (NN) analysis basen on amide I absorbtion band as reported previously.[8] Type I DM was induced by the administration of streptozotocin (STZ). STZ is a commonly used agent in the induction of DM by the specific destruction of pancreatic β-cells, which corresponds with type I DM conditions.[36] Its effective usage to induce type I DM in animal models has been proven in the literature since treatment with insulin recovers almost all alterations caused by STZ-induced DM, i.e., the altered parameters of calcium sparks in cardiomyocytes,[37] impaired endothelium-dependent relaxation in the rat aorta,[38] impaired mechanical properties and thermal stability of rat tail tendon,[39] altered substance *P* levels in sciatic nerves of rats,[40] and alterations in tissue antioxidant status.[41]

2 Materials and Methods

2.1 *Reagents*

STZ (S0130), citric acid (251275), sodium citrate monobasic (71497), and sodium selenite (S5261) were purchased from Sigma (Sigma Chemical Company, Saint Louis, Missouri, USA) at the highest grade of purity available varying in between 98% and 99.5%.

2.2 *Rat Model of Type I DM and Selenium Administration*

Male Wistar rats (200 to 250 g) were randomly selected and fed with a standard maintenance diet *ad libitum*. The rats were kept at an ambient air temperature of 22°C and with a 12-h light, 12-h dark cycle. All of the procedures used in this study were approved by University Ethics Committee. The rats were divided into four groups, namely control ($n = 6$), diabetic ($n = 6$), low dose selenium treated diabetic ($n = 5$), and high-dose selenium treated diabetic ($n = 4$). DM was induced by a single intraperitoneal (i.p.) dose of STZ (50 mg/kg) injection dissolved in 0.05 mol/L citrate buffer (pH 4.5). Control rats received a single i.p. dose of citrate buffer (0.05 mol/L, pH 4.5). Six hours after STZ administration, the diabetic group received a single dose of 5% dextrose solution in order to prevent mortality due to hypoglycemic shock. Blood glucose levels were measured after three days, and those with glucose levels below 300 mg/dl were not considered as diabetic. After the induction of DM, the animals in the selenium treated groups were injected with 1 μmol/kg/day (low dose) and 25 μmol/kg/day (high dose) sodium selenite i.p. for 5 weeks. During this period, physiological saline solution was administered to the rats in diabetic and control group. At the end of the fifth week, the rats were decapitated; their livers were removed and kept at −80°C until use.

2.3 *Sampling for FTIR Imaging Studies*

Twelve-μm thick tissue sections from the livers were obtained using a cryotome (Shandon, USA) and were directly transferred onto commercially available IR transparent calcium fluoride (CaF_2) windows (Korth Kristalle GmbH, Altenholz, Kiel, Germany) and allowed to dry at room temperature overnight. Two different regions per section were selected for FTIR imaging studies from each group.

2.4 *FTIR Imaging*

FTIR images were acquired using an FTIR spectrometer (model 670; Agilent Technologies Inc., Santa Clara, CA, USA) coupled to an infrared microscope (model 620; Agilent) using a $15\times$ objective and fitted with a liquid-nitrogen-cooled MCT 64×64 element-focal-plane array detector. The FTIR system was controlled by IBM compatible PC running Resolution Pro software (Agilent). The absorbance spectra were acquired in transmittance mode at a spectral resolution of 8 cm^{-1} with 64 scans co-added. The system enabled 4096 spectra to be acquired from a sample area of approximately 350 μm^2 in 2 min. Each pixel corresponded to an area of 5.5×5.5 μm^2. Background scans were acquired and subtracted from the sample spectrum.

2.5 *Data Processing and Analysis for FTIR Microspectroscopy*

The resulting FTIR images were processed using CYTOSPEC v.1.4.02 [http://www.cytospec.com] imaging software packages. A quality test of the raw spectral data was performed to check for water vapor and for specific bands of the tissue-freezing medium. Low-absorbance spectra with poor signal-to-noise ratios in spectroscopic images were removed, since they correspond to positions outside the tissue, near holes, fissures, or margins. The thickness quality test was used to eliminate spectra of samples that were too thick or thin. The intensity of the amide I band was used to determine the quality of sections. All spectra that passed the quality test were subsequently offset corrected and baseline corrected. The chemical images for visual presentation were constructed based on band area ratios.

Processed spectral data sets were used to obtain average spectra, which were then imported into OPUS 5.5 software (Bruker Optics, Germany) and further data analyses of band areas were performed using this program. In order to understand whether scattering phenomenon interferes with the data, resonant Mie scattering correction was applied to the average spectra imported from the images. Since similar spectra were obtained after this correction, native spectra were used for further data analysis without Mie scattering correction. Band area values were calculated using a linear baseline from 3100 to 2750 cm^{-1} and from 1780 to 950 cm^{-1} for C-H stretching and fingerprint regions, respectively. The lipid to protein ratio was obtained by calculating the ratio of the area of the C-H stretching region (integrated area under the region from 3000 to 2800 cm^{-1}) to the area under the amide I band (integrated area under the region from 1700 to 1600 cm^{-1}). The C-H

stretching region contains a band that mainly originates from proteins (CH_3 symmetric stretching band).[8,42] However, since this band is very weak, the C-H region can be considered as a lipid region.[43] In order to quantitatively investigate the changes in glycogen content with respect to protein content; the area under the region from 1180 to 975 cm^{-1} was divided to the area of the amide II band (integrated area under the region from 1590 to 1480 cm^{-1}) of proteins. To obtain information on the variation in protein structure, the amide I/amide II ratio was calculated by dividing the area under the amide I band to that of amide II band.[44,45]

Alterations in protein secondary structures were predicted using NN models, which have been obtained to predict α-helix and β-sheet contents in 1700 to 1600 cm^{-1} spectral region of the FTIR spectra, as described before.[46] Two-layer NNs, having one hidden layer and one output layer, were first trained with a reference data set containing FTIR spectra of 18 water soluble proteins with known secondary structure.[46] In order to obtain NNs that can generalize well when trained with such a small set of reference data, the number of inputs had to be reduced. Discrete cosine transform (DCT) of the normalized spectra was obtained for the purpose of compaction of data. Bayesian regulation was used to train the NNs. The training process yielded NN models whose structures were optimized in terms of the number of inputs, number of hidden units, and the threshold for sum-squared errors. The resulting optimized network for alpha-helix structure had 12 inputs (12 DCT coefficients), a hidden layer with two neurons, and an output layer with one neuron. For beta-sheet structure the network had 19 inputs, two hidden neurons, and one output neuron. For both structures, a sigmoid transfer function was used in each layer. To predict the secondary structure contents of the new proteins from the measured FTIR spectrum, the NNs were driven by the required number of DCT coefficients of the normalized spectrum. To increase prediction accuracy, the above-described procedure was repeated 200 times and the most likely value of the output (the mode of the histogram) was accepted as the prediction.

For principal component analysis (PCA), the average spectra extracted from images of each group were imported into MATLAB (Mathworks Inc.) and PCA was performed within the regions from 1200 to 1050 cm^{-1} (glycogen) and from 1600 to 1500 cm^{-1} (amide II) using the average absorbance spectra and in the region from 1700 to 1600 cm^{-1} (amide I) utilizing the first derivative spectra, as described previously.[47] The PCA software was developed in the laboratory of Eric Goormaghtigh, who generously supplied it to us. PCA is a statistical method that enables the reduction of data. The method transforms the original large set of variables to a new set of uncorrelated small number of variables called principal components (PCs). These components are independent of each other, and the first PC has the maximum variance. The reduction of data provides a new coordinate system where axes (PCs) represent the characteristic structure information of the data along different eigenvectors retaining as much of the information in the original variables as possible. This enables the spectra to be described as a function of specific properties, and not a function of intensities.[47] The outcome of the analysis can be presented as scatter plots.

2.6 *Statistics*

The results were expressed as means ± standard error of mean for each group. The differences in the means of the groups were compared by student t-test using the Minitab Statistical Software Release 3.0 program (State College, PA, USA). p values equal to or less than 0.05 were accepted as significantly different from the control group. The degree of significance was denoted as $p < 0.05*$, $p < 0.01**$, $p < 0.001***$.

3 Results and Discussion

Growing evidence emphasizes the relation between alterations in protein structure and pathogenesis of many disorders[1,2] including type II DM.[3,4] Accordingly, this current study was conducted to assess the protein secondary structural changes in STZ-induced type I diabetic rat liver, together with the alterations in macromolecular content, using FTIR microspectroscopy. In addition, the role of selenium supplementation in the recovery of diabetes-induced alterations in protein structure and macromolecular content with respect to that of proteins, such as lipid to protein and glycogen to protein ratios, was investigated.

Figure 1 shows the average FTIR spectra of control liver tissues in 4000 to 900 cm^{-1} region. The main bands are labeled in the figure and the band assignments are given in Table 1. Figure 2 shows the avarage FTIR spectra of control, diabetic, low- and high-dose selenium treated diabetic rat liver tissues in 1800 to 900 cm^{-1} region. The figure reveals there are prominent differences between the avarage spectra belonging to the different groups, especially in 1200 to 1050 cm^{-1} region. Subtle changes in band shape, band position, band intensity, and/or area of vibrational bands represent changes in concentration, composition, and structure of biomolecules, respectively. Based on these spectral differences, the PCA analysis of data differentiated the control from the diabetic group both in 1200 to 1050 cm^{-1} and amide regions (Fig. 3).

The relative concentrations of the functional groups belonging to different macromolecules were determined by measuring the area under the related absorption bands.[5,6,42] Figure 4 shows the photomicrograph of unstained tissue (a) and the chemical images demonstrating the distribution of (b) lipid to protein (amide I) ratio (c) glycogen to protein (amide II) ratio, and (d) amide I/amide II ratio of control, diabetic, low and high dose selenium treated diabetic groups, respectively. The changes in the ratio of the band areas of the mentioned infrared absorptions are shown in Table 2. The values of lipid/protein and glycogen/protein ratios were significantly decreased ($p < 0.001$) for the diabetic group compared to the control [Table 2,

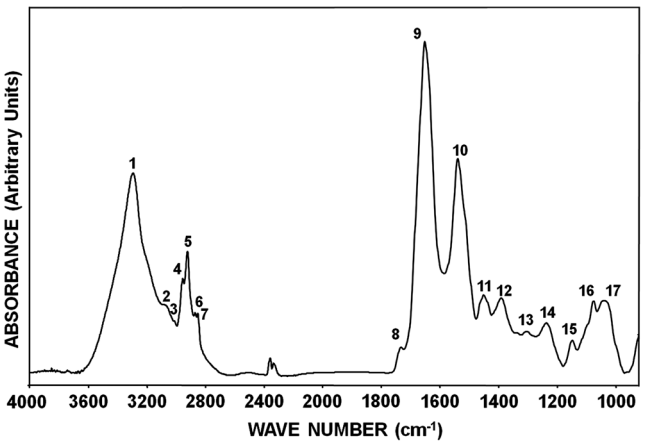

Fig. 1 The average micro-FTIR spectra of control liver tissues in 4000 to 900 cm^{-1} region.

Table 1 Band assignments of major absorptions in IR spectra of control liver tissue in 4000 to 900 cm^{-1} region.

Peak No	Wavenumber (cm^{-1})	Definition of the spectral assignment[8,12,42,48,49]
1	3296	Amide A: mainly N-H stretching of proteins
2	3081	Amide B: N-H stretching of proteins
3	3016	Olefinic = CH stretching vibration: unsaturated lipids, cholesterol esters
4	2958	CH_3 antisymmetric stretch: lipids, proteins
5	2925	CH_2 antisymmetric stretch: mainly lipids
6	2873	CH_3 symmetric stretch: mainly proteins
7	2855	CH_2 symmetric stretch: mainly lipids
8	1735	Saturated ester C = O stretch: phospholipids, cholesterol esters
9	1655	Amide I: protein (80% C = O stretching, 10% N-H bending, 10% C-N stretching)
10	1542	Amide II: protein (60% N-H bending, 40% C-N stretching)
11	1455	CH_2 bending: mainly lipids, protein
12	1395	COO^- symmetric stretch: fatty acids and amino acids
13	1305	Protein (amide III)
14	1239	PO_2^- antisymmetric stretch: nucleic acids, phospholipids
15	1152	CO-O-C antisymmetric stretching: glycogen and nucleic acids
16	1079	PO_2^- symmetric stretch: nucleic acids, phospholipids
17	1040	C-O stretching: polysaccharides, glycogen

Fig. 4(b) to 4(c)]. This decrease might be due to either the prominent increase in protein or decrease in lipid and glycogen content as also observed in the current study (data not shown).

The changes in protein content and structure can be monitored by analyzing the main protein bands, amide I and II, which are centered at 1655 and 1542 cm^{-1}, respectively.[31] Amide I band originates mainly due to the C = O stretching (80%), with little contribution from the C-N stretching vibrational modes (10%) that are weakly coupled with the N-H bending (10%) of the polypeptide and protein backbone; whereas amide II band is assigned to the N-H bending (60%) and the C-N stretching (40%) modes of proteins (Table 1).[48] Since these bands originate from different vibrations of protein structure and depend on the protein structural composition,[42] amide I (mainly C = O stretching) to amide II (mainly N-H bending) area/intensity ratio can be used to obtain a rough estimation of the presence of possible changes in protein structure and conformation.[42,44,45,50] There was a significant decrease ($p < 0.01$) in the ratio of the areas of amide I to amide II bands in the diabetic group [Fig. 4(d)], revealing a change in protein structure in diabetic liver. Recent studies also reveal that diseased tissues show a change in the percentage of protein secondary structures and/or a reduced ratio of amide I to amide II when compared with normal tissue.[42,51] In order to better understand and comment on the changes in protein secondary structure, a more precise method, namely NN approach,[7,42,52] which is based on amide I absorption, (1700 to 1600 cm^{-1}) was used in the prediction of diabetes-induced protein secondary structure alterations and to investigate the effect of selenium treatment on protein secondary structure. NN results revealed a significant decrease in α-helical ($p < 0.01$) and the increase in total β-sheet content ($p < 0.05$) in diabetic group with respect to the control group (Table 3).

These results demonstrated a transition in protein conformation in diabetic liver from α-helical to β-sheet structures, which

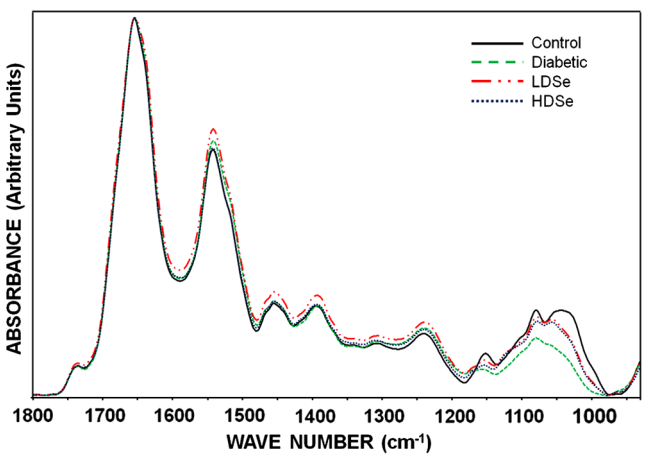

Fig. 2 The average micro-FTIR spectra of control, diabetic, low-dose selenium (LDSe), and high-dose selenium (HDSe) treated diabetic liver tissues in 1800 to 900 cm^{-1} region (spectra were normalized with respect to amide I band).

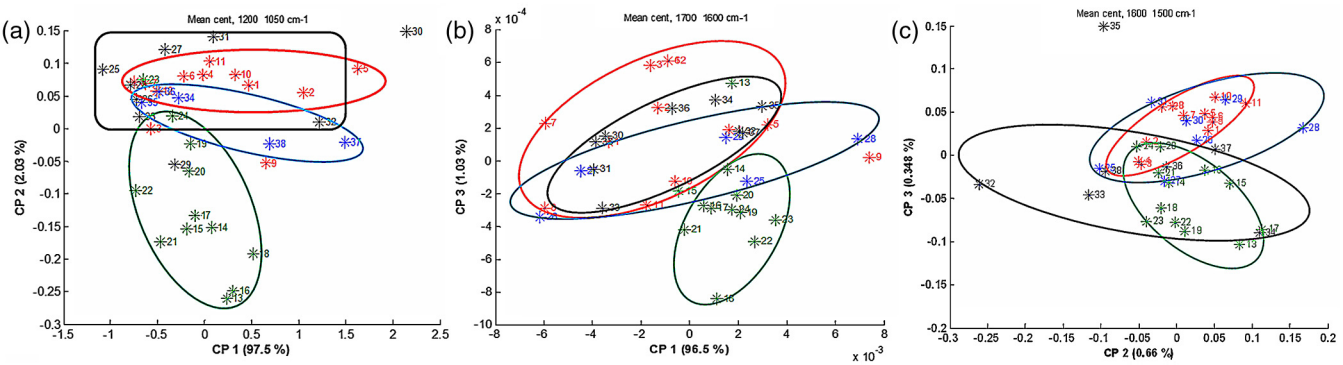

Fig. 3 PCA analysis of the FTIR spectra of liver tissues in control (red), diabetic (green), low-dose treated diabetic (black), and high-dose treated diabetic (blue) groups in (a) 1200 to 1050 cm^{-1} (glycogen), (b) 1700 to 1600 cm^{-1} (amide I), (c) 1600 to 1500 cm^{-1} (amide II) regions. Average absorbance spectra were used to construct the PCs except for amide I region, where first dervative spectra were utilized. The percentages between brackets represent the proportion of variance held in the principal components.

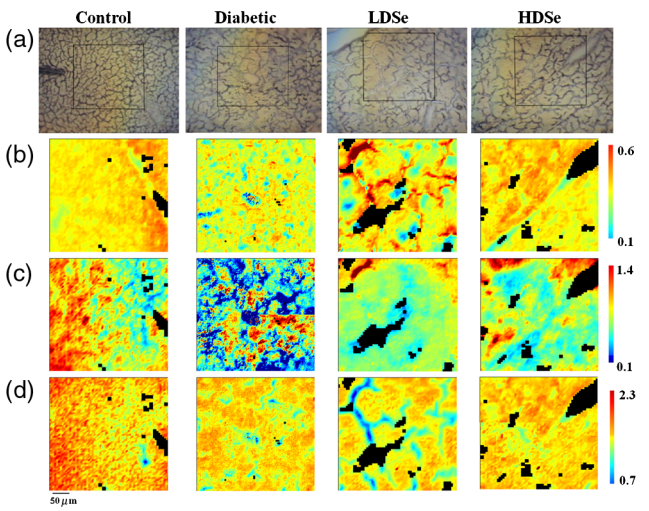

Fig. 4 Photomicrograph of unstained tissue (the black box outlines mapped area) (a), and FTIR chemical images (image size 64 × 64 pixel, the measurement area 350 × 350 μm) demonstrating the distribution of lipid to protein ratio (b), glycogen to protein ratio (c), and amide I/amide II ratio (d) of control, diabetic, low dose selenium (LDSe) and high-dose selenium (HDSe) treated diabetic liver sections. Colorbar indicates ratio gradient from low to high. Some pixels were omitted after quality testing (shown in black). Absorbance intensity ratios of FTIR images are proportional to color changes as shown in the color bar: blue (lowest) and red (the highest). Scale bar: 50 μm.

is a generally observed phenomenon in protein conformational diseases[53] together with an increase in cross β-structures in proteins.[54,55] A similar increase in β-sheet structures was also observed in protein deposits in the islets of pancreas tissues from autopsies of type II DM patients; however proteins in the areas of the pancreas without amyloid deposits had predominantly an α-helical structure.[56] Apart from pancreatic tissue, Mahmoud[57] reported a higher content of β-sheet structures, together with a reduced content of β-turns, in erytrocyte membranes of type II DM subjects having higher glycemic levels. This shift from α-helical to β-sheet structures in protein conformation was also previously reported in STZ-induced diabetic rat skeletal muscle[8] and heart.[6,7] Taken together, these findings demonstrate that the alterations in protein structure in DM take place not only in the pancreas but also in different tissues. These alterations can originate from structural rearrangements of already existing proteins or may be a result of the expression of new types of proteins with altered structure.[7] One possible mechanism for the structural rearrangements in proteins may be the increase in lipid peroxidation in diabetes, as malonaldehyde, a lipid peroxidation by-product, was reported to alter protein structure.[58] Since protein insolubility increases with the increase in β-sheet content,[57] it should also be noted that the changes in protein structure and the increase in β-sheet structures may lead to the denaturation and aggregation of proteins in diabetic liver; however, further studies are needed for the identification of any possible protein deposits.

In recent years, research has been focused on the antidiabetic action of selenium. In most of the studies, daily selenate or

Table 2 Changes in ratio of areas for control, diabetic, low-dose selenium (LDSe) treated diabetic, and high-dose selenium (HDSe) treated diabetic livers.

Band ratio	Control ($n = 6$)	Diabetic ($n = 6$)	LDSe ($n = 5$)	HDSe ($n = 4$)
Lipid to protein (Lipid/Amide I)	0.48 ± 0.01	0.43 ± 0.01^{b}	0.51 ± 0.02	0.49 ± 0.01
Glycogen/Amide II	1.17 ± 0.11	0.49 ± 0.0^{b}	0.84 ± 0.17	0.85 ± 0.11
Amide I/Amide II	2.08 ± 0.03	1.91 ± 0.02^{c}	1.91 ± 0.03^{c}	2.02 ± 0.05

The values are the mean ± standard error of mean for each group. Comparisons were performed by the t-test.
[a]The degree of significance was denoted as $p < 0.05$.
[b]The degree of significance was denoted as $p < 0.001$.
[c]The degree of significance was denoted as $p < 0.01$.

Table 3 The results of the changes in protein secondary structure for control, diabetic, low-dose selenium (LDSe) treated diabetic, and high-dose selenium (HDSe) treated diabetic livers obtained from NN predictions based on FTIR data in 1600 to 1700 cm^{-1} spectral region (amide I band).

Functional groups	Control ($n = 6$)	Diabetic ($n = 6$)	LDSe ($n = 5$)	HDSe ($n = 4$)
α-helix	48.05 ± 0.88	43.32 ± 1.54^{b}	41.52 ± 1.82^{a}	45.29 ± 1.21
β-sheet	21.86 ± 0.54	24.02 ± 0.75^{a}	24.59 ± 1.08^{a}	22.95 ± 0.81

The values are the mean ± standard error of mean for each group. Comparisons were performed by the t-test.
[a]The degree of significance was denoted as $p < 0.05$.
[b]The degree of significance was denoted as $p < 0.01$.

selenite administration effectively improved glucose homeostasis in rats with STZ-induced type I DM with considerable changes in antioxidant enzyme activities and the expression of glycolytic and gluconeogenic enzymes.[23,59] It was also reported to improve whole-body insulin sensitivity in type II diabetic db/db mice by significantly increasing the total liver lipid and liver triglyceride concentration.[18] The findings in this current study revealed an increase in lipid to protein and glycogen to protein ratios upon selenite treatment, which indicates a recovery effect of selenium (Table 2). This might be related to an increase in the lipid and glycogen contents. Indeed in the current study, we observed an increase in the lipid content from 17.41 ± 0.37 in diabetic group to 18.78 ± 1.14 in low-dose selenium and to 20.33 ± 1.40 in high dose selenium treated diabetic groups. There was also an increase in glycogen content revealed by the calculated glycogen areas as 10.38 ± 0.66 in diabetic, 15.50 ± 4.43 in low-dose selenium and 17.45 ± 3.31 in high-dose selenium-treated diabetic groups. It is interesting that, although no recovery effect of selenium was observed in the lipid content, the ratio of lipid to protein content was restored to the level of control (Table 2). This is an important observation because the lipid to protein ratio is a critical factor directly affecting the preferred macromolecular distribution for proper membrane functioning.[8]

Although selenium compounds were reported to have antidiabetic effects, there are some conflicting results in the literature as recent epidemiological studies point out that persistent high-plasma selenium levels can increase the prevelance of type II DM and hyperglycemia.[19,24,25] It is well established that antioxidants may have toxic effects at high doses; for instance, administration of higher doses of selenite (500 μM) causes degeneration and necrosis of hepatocytes leading to the impairment of metabolic functions of the liver.[60] The recommended uptake for the physiological action of selenium is 0.15 to 0.30 mg/kg dietary dry matter for animals, and the minimum lethal dose for selenium compounds varies from 2.0 to approximately 5.0 mg/kg body weight.[26]

It was reported that signs of toxicity of selenium/sodium selenite are observed when doses above 5 mg/kg are administered to animals.[61,62] The results of this current study revealed that the 1 μmol/kg dose (corresponding approximately to 0.17 mg/kg, physiological dose) of selenium recovers diabetes-induced changes in lipid to protein and glycogen to protein ratios [Table 2, Fig. 4(b) and 4(c)]. This dose, however, was not sufficient to restore the alterations in protein secondary structure (Table 3). Nevertheless, 25 μmol/kg dose (corresponding approximately to 4.3 mg/kg, around the limit of minimum lethal dose) selenium administration restored the changes in lipid to protein and glycogen to protein ratios together with the alterations in protein secondary structure [Table 2, Table 3, Fig. 4(b) to 4(d)]. These findings can also be observed in the PCA score plot of the region from 1200 to 1050 cm^{-1} originating from glycogen [Fig. 3(a)], which reveal that selenium-treated groups are segregated from diabetic group and tend to be grouped more close to the control. In addition, the PCA analysis of the amide I and II region [Fig. 3(b) and 3(c)] demonstrated that both doses of selenium have restoring effect, more prominently at high dose. This recovery effect of selenium on protein structure at a higher dose might be due to its effective antioxidant action on lipid peroxidation, since the relation between lipid peroxidation and protein secondary structural alterations has been previously reported.[58] Supporting this observation, Sheng et al.[63] has also observed that a similar high dose of selenium (4 mg/kg) treatment decreased lipid peroxidation level by increasing GSH-Px activity in the red blood cells of alloxan induced-diabetic mice.

4 Conclusion

This study was the first to report the alterations in protein structure in STZ-induced diabetic rat liver tissues, where a decrease in α-helical structures together with an increase in β-sheet content was observed. This is one of the common characteristics of conformational diseases, which eventually lead to protein aggregation. In order to depict any possible protein deposits, further studies are needed. The findings of this study also suggest that, although supplementation of selenium at a low dose (physiological dose) was able to recover diabetes-induced changes in lipid to protein and glycogen to protein ratios, it was not sufficient to reinstate the alterations in protein secondary structure. On the other hand, higher doses of selenium was needed to achieve a satisfactory antioxidant effect to restore normal protein structure together with the restoring effect both in lipid to protein and glycogen to protein ratios.

Acknowledgments

This work was supported through DAAD (German Academic Exchange Service). We would like to give our special thanks to Prof. Dr. Eric Goormaghtigh, who generously provided us the PCA analysis software developed in his laboratory and kindly adapted the program to our spectral data. We would also like to thank to Prof. Dr. Peter Gardner for providing us the resonant Mie scattering correction software.

References

1. S. Y. Lin and H. L. Chu, "Fourier transform infrared spectroscopy used to evidence the prevention of β-sheet formation of amyloid β(1–40) peptide by a short amyloid fragment," *Int. J. Biol. Macromol.* **32**(3–5), 173–177 (2003).

2. M. M. Apetri et al., "Secondary structure of α-synuclein oligomers: characterization by raman and atomic force microscopy," *J. Mol. Biol.* **355**(1), 63–71 (2006).
3. A. Clark et al., "Pancreatic pathology in noninsulin dependent diabetes (NIDDM)," *Diabetes Res. Clin. Pract.* **28**(Suppl.), S39–S47 (1995).
4. R. L. Hull et al., "Islet amyloid: a critical entity in the pathogenesis of type 2 diabetes," *J. Clin. Endocrinol. Metab.* **89**(8), 3629–3643 (2004).
5. F. Severcan, N. Kaptan, and B. Turan, "FTIR spectroscopic investigation of diabetic rat heart crude membranes," *Spectros. Int. J.* **17**(2–3), 569–577 (2003).
6. N. Toyran et al., "Early alterations in myocardia and vessels of the diabetic rat heart: an FTIR microspectroscopic study," *Biochem. J.* **397**(3), 427–436 (2006).
7. N. Toyran et al., "Investigation of diabetes-induced effect on apex of rat heart myocardium by using cluster analysis and neural network approach: an FTIR study," *Spectros. Int. J.* **21**(5–6), 269–278 (2007).
8. O. Bozkurt, M. Severcan, and F. Severcan, "Diabetes induces compositional, structural and functional alterations on rat skeletal soleus muscle revealed by FTIR spectroscopy: a comparative study with EDL muscle," *Analyst.* **135**(12), 3110–3119 (2010).
9. S. R. Stapleton, "Selenium: an insulin-mimetic," *Cellul. Mol. Life Sci.* **57**(13–14), 1874–1879 (2000).
10. A. M. Brands et al., "Diabetic encephalopathy: an underexposed complication of diabetes mellitus," *Ned Tijdschr Geneeskd.* **147**(1), 11–14 (2003).
11. F. Severcan et al., "Rapid monitoring of diabetes-induced lipid peroxidation by FTIR spectroscopy," *Anal. Biochem.* **339**(1), 36–40 (2005).
12. F. Severcan et al., "FTIR spectroscopy in diagnosis of diabetes in rat animal model," *J. Biophoton.* **3**(8–9), 621–631 (2010).
13. O. Bozkurt, M. D. Bilgin, and F. Severcan, "The effect of diabetes mellitus on rat skeletal extensor digitorum longus muscle tissue: an FTIR study," *Spectros. Int. J.* **21**(3), 151–160 (2007).
14. H. Boyar, B. Turan, and F. Severcan, "FTIR spectroscopic investigation of mineral structure of streptozotocin induced diabetic rat femur and tibia," *Spectros. Int. J.* **17**(2–3), 627–633 (2003).
15. A. A. Hassan et al., "The effect of diabetes on sexual behavior and reproductive tract function in male rats," *J. Urol.* **149**(1), 148–154 (1993).
16. G. Sadi, O. Yılmaz, and T. Guray, "Effect of vitamin C and lipoic acid on streptozotocin-induced diabetes gene expression:mRNA and protein expressions of Cu-Zn SOD and catalase," *Mol. Cell. Biochem.* **309**(1–2), 109–116 (2008).
17. I. G. Obrosova et al., "Early oxidative stress in the diabetic kidney: effect of DL-alpha-lipoic acid," *Free Radical Biol. Med.* **34**(2), 186–195 (2003).
18. A. S. Mueller and J. Pallauf, "Compendium of the antidiabetic effects of supranutritional selenate doses. In vivo and in vitro investigations with type II diabetic db/db mice," *J. Nutr. Biochem.* **17**(8), 548–560 (2006).
19. H. Steinbrenner et al., "High selenium intake and increased diabetes risk: experimental evidence for interplay between selenium and carbohydrate metabolism," *J. Clin. Biochem. Nutr.* **48**(1), 40–45 (2011).
20. J. T. Salonen et al., "Association between cardiovascular death and myocardial infarction and serum selenium in a matched-pair longitudinal study," *Lancet* **320**(8291), 175–179 (1982).
21. J. Chen and M. J. Berry, "Selenium and selenoproteins in the brain and brain diseases," *J. Neurochem.* **86**(1), 1–12 (2003).
22. P. Brenneisen, H. Steinbrenner, and H. Sies, "Selenium, oxidative stress, and health aspects," *Mol. Aspects Med.* **26**(4–5), 256–267 (2005).
23. D. J. Becker et al., "Oral selenate improves glucose homeostasis and partly reverses abnormal expression of liver glycolytic and gluconeogenic enzymes in diabetic rats," *Diabetologia* **39**(1), 3–11 (1996)
24. S. Stranges et al., "Effects of long-term selenium supplementation on the incidence of type II diabetes: a randomized trial," *Ann. Intern. Med.* **147**(4), 217–223 (2007).
25. J. Bleys, A. Navas-Acien, and E. Guallar, "Serum selenium and diabetes in US adults," *Diabetes Care* **30**(4), 829–834 (2007).
26. A. S. Mueller et al., "Selenium and diabetes: an enigma?," *Free Radical Res.* **43**(11), 1029–1059 (2009).
27. C. Krafft et al., "Disease recognition by infrared and Raman spectroscopy," *J. Biophoton.* **2**(1–2), 13–28 (2009).
28. D. C. Fernandez et al., "Infrared spectroscopic imaging for histopathological recognition," *Nat. Biotechnol.* **23**(4), 469–474 (2005).
29. S. Y. Lin, M. J. Li, and W. T. Cheng, "FTIR and Raman vibrational microspectroscopies used for spectral biodiagnosis of human tissues," *Spectros. Int. J.* **21**(1), 1–30 (2007).
30. D. Naumann, "FT-infrared and FT-Raman spectroscopy in biomedical research," *Appl. Spectrosc. Rev.* **36**(2&3), 239–298 (2001).
31. P. Haris and F. Severcan, "FTIR spectroscopic characterization of protein structure in aqueous and non-aqueous media," *J. Mol. Catal. B Enzym.* **7**(1–4), 207–221 (1999).
32. T. Meyer et al., "Nonlinear microscopy, infrared, and Raman microspectroscopy for brain tumor analysis," *J. Biomed. Opt.* **16**(2), 021113 (2011).
33. A. C. Leskovjan, A. Kretlow, and L. M. Miller, "Fourier transform infrared imaging showing reduced unsaturated lipid content in the hippocampus of a mouse model of Alzheimer's disease," *Anal. Chem.* **82**(7), 2711–2716 (2010).
34. A. Boskey and N. C. Pleshko, "FTIR imaging of native and tissue-engineered bone and cartilage," *Biomaterials* **28**(15), 2465–2478 (2007).
35. S. Haman Bayarı et al., "Synchrotron FTIR microspectroscopic analysis of necrotic bone," *Spectros. Int. J.* **21**(4), 227–234 (2007).
36. X. P. Zhang and B. K. H. Tan, "Antihyperglycaemic and antioxidant properties of andrographis paniculata in normal and diabetic rats," *Clin. Exp. Pharmacol. Physiol.* **27**(5–6), 358–363 (2000).
37. N. Yaras et al., "Effects of diabetes on ryanodine receptor ca release channel (RyR2) and Ca^{2+} homeostasis in rat heart," *Diabetes* **54**(11), 3082–2088 (2005).
38. T. Kobayashi and K. Kamata, "Effect of chronic insulin treatment on NO production and endothelium-dependent relaxation in aortae from established STZ-induced diabetic rats," *Atherosclerosis* **155**(2), 313–320 (2001).
39. T. T Andreassen, K. Seyer-Hansen, and A. J. Bailey, "Thermal stability, mechanical properties and reducible cross-links of rat tail tendon in experimental diabetes," *Biochim. Biophys. Acta* **677**(2), 313–317 (1981).
40. P. Fernyhough et al., "Deficits in sciatic nerve neuropeptide content coincide with a reduction in target tissue nerve growth factor messenger RNA in streptozotocin-diabetic rats: effects of insulin treatment," *Neuroscience* **62**(2), 337–344 (1994).
41. S. A. Wohaieb and D. V. Godin, "Alterations in free radical tissue-defense mechanisms in streptozotocin-induced diabetes in rat: effects of insulin treatment," *Diabetes* **36**(9), 1014–1018 (1987).
42. G. Cakmak et al., "Screening of protective effect of amifostine on radiation-induced structural and functional variations in rat liver microsomal membranes by FTIR spectroscopy," *Anal. Chem.* **83**(7), 2438–2444 (2011).
43. S. Garip, A. C. Gozen, and F. Severcan, "Use of Fourier transform infrared spectroscopy for rapid comparative analysis of bacillus and micrococcus isolates," *Food chem.* **113**(4), 1301–1307 (2009).
44. S. B. Dev, J. T. Keller, and C. K. Rha, "Secondary structure of 11 S globulin in aqueous solution investigated by FTIR derivative spectroscopy," *Biochim. Biophys. Acta* **957**(2), 272–280 (1988).
45. K. P. Ishida and P. R. Griffiths, "Comparison of the amide i/ii intensity ratio of solution and solid-state proteins sampled by transmission, attenuated total reflectance, and diffuse reflectance spectrometry," *Appl. Spectros.* **47**(5), 584–589 (1993).
46. M. Severcan, F. Severcan, and I. P. Haris, "Using artificially generated spectral data to improve protein secondary structure prediction from FTIR spectra of proteins," *Anal. Biochem.* **332**(2), 238–244 (2004).
47. R. Gasper et al., "IR spectroscopy as a new tool for evidencing antitumor drug signatures," *Biochim. Biophys. Acta.* **1788**(6), 1263–1270 (2009).
48. B. Stuart, *Biological Applications of Infrared Spectroscopy*, John Wiley and Sons, England (1997).
49. Z. Movasaghi, S. Rehman, and I. Rehman, "Fourier transform infrared (FTIR) spectroscopy of biological tissues," *Appl. Spectros. Rev.* **43**(2), 134–179 (2008).
50. A. Dogan, G. Siyakus, and F. Severcan, "FTIR spectroscopic characterization of irradiated hazelnut (*Corylus avellana* L.)," *Food Chem.* **100**(3), 1106–1114 (2007).

51. Szczerbowska-Boruchowska et al., "Biomolecular investigation of human substantia nigra in Parkinson's disease by synchrotron radiation Fourier transform infrared microspectroscopy," *Arch. Biochem. Biophys.* **459**(2), 241–248 (2007).
52. B. Elibol-Can et al., "The effects of short-term chronic ethanol intoxication and ethanol withdrawal on the molecular composition of the rat hippocampus by FTIR spectroscopy," *Alcohol Clin. Exp. Res.* **35**(11), 2050–2062 (2011).
53. G. Liu et al., "Mechanistic studies of peptide self-assembly: transient α-helices to stable β-sheets," *J. Am. Chem. Soc.* **132**(51), 18223–18232 (2010).
54. M. von Bergen et al., "Tau aggregation is driven by a transition from random coil to beta sheet structure," *Biochim. Biophys. Acta.-Mol. Basis Dis.* **1739**(2–3), 158–166 (2005).
55. J. C. Lin and H. L. Liu, "Protein conformational diseases: from mechanisms to drug designs," *Curr. Drug Discov. Tech.* **3**(2), 145–153 (2006).
56. J. Miklossy et al., "Beta amyloid and hyperphosphorylated tau deposits in the pancreas in type 2 diabetes," *Neurobiol. Aging* **31**(9), 1503–1515 (2010).
57. S. S. Mahmoud, "The impact of elevated blood glycemic level of patients with type ii diabetes mellitus on the erythrocyte membrane: FTIR study," *Cell Biochem. Biophys.* **58**(1), 45–51 (2010).
58. S. J. Li and A. J. King, "Structural changes of rabbit myosin subfragment 1 altered by malonaldehyde, a byproduct of lipid oxidation," *J. Agrig. Food. Chem.* **47**(8), 3124–3129 (1999).
59. B. Mukherjee et al., "Novel implications of the potential role of selenium on antioxidant status in streptozotocin-induced diabetic mice," *Biomed. Pharmacother.* **52**(2), 89–95 (1998).
60. M. Roden et al., "Metabolic effect of sodium selenite: insulin-like inhibition of glucagon-stimulated glycogenolysis in the isolated perfused rat liver," *Hepatology* **22**(1), 169–174 (1995).
61. A. W. Halverson, I. S. Palmer, and P. L. Guss, "Toxicity of selenium to postweanling rats," *Toxicol. Appl. Pharmacol.* **9**(3), 477–484 (1966).
62. National Research Council (NRC) "SELENIUM," *Mineral tolerance of domestic animals*, pp. 392–420, The National Academies Press, Washington, DC (1980).
63. X. Q. Sheng, K. X. Huang, and H. B. Xu, "New experimental observation on the relationship of selenium and diabetes mellitus," *Biol. Trace Elem. Res.* **99**(1–3), 241–253 (2004).